

Crystalline quality in aluminium single crystals, characterized by X-Ray diffraction and Rocking-Curve analysis

G. Orr*, G. Golan†

*Department of Physics, Ariel University, Ariel 40700, Israel

†Department of Electrical Engineering, Ariel University, Ariel 40700, Israel

Abstract—Aluminum single crystals are tested using X-Ray Bragg diffraction, which may have applications in microscopy and electronics fabrication industry. Yet, their efficiency for x-ray beam diffraction depends on the accurate crystal orientation, the microstructure and imperfections. Moreover, the final sample that is formed from the as-grown crystal by cutting, grinding, polishing and chemical etching, introduces various surface defects that penetrate deep into the crystal affecting its natural structure. Defect penetration is attributed to the fact that ultra-pure aluminum single crystals are soft and ductile with a hardness in the range of 2~2.5 mho. This leads to lattice deformation, resulting in a deviation from the crystallographic orientation of the final device, affecting the diffraction intensity and an apparent shift in the Bragg angle. In this work we investigate the influence of processing aluminum single crystals by mechanical and chemical means using XRD and Rocking-Curve broadening as a quantitative indication concerning the depth of the damage. This is a preliminary step in supporting future work on the study of electrical conduction in aluminum single crystals. Supplementing electrical conductivity measurements of aluminum, quality assessment of defects in front cell aluminum conductors can assist in designing novel low resistance aluminum conductors replacing the currently widely used and relatively rare silver.

Index Terms—Aluminum Single crystals, X-Ray Diffraction, Crystal Orientation, Imperfections, PV cells.

I. INTRODUCTION

Conduction in elemental metallic crystals is still intensively investigated [1] and is of great technological importance in modern microelectronics and photovoltaics. Of the FCC metallic crystal family, aluminum is widely used in modern microelectronic fabrication as it is a relatively abundant, acceptable conductor which to some extent is superior to copper for it does not diffuse into silicon at operating temperatures ($< 450^\circ C$). That said, with all the complications copper adds to device manufacturing aluminum's conductivity is only 63% compared to the conductivity of copper ($0.0172 \Omega \cdot mm^2/m$ vs. $0.0282 \Omega \cdot mm^2/m$). Thus increasing aluminum's

conductivity has its merits. Current photovoltaic cell bus bar and finger technology consists of silver screen printing thus relying on a relatively rare and expensive metal. Replacing the silver with an abundant metal may reduce the production costs considerably, therefore given the considerations above aluminum is a good candidate. Depositing the aluminum on the silicon substrate does not require a conductive seed layer or a Ni barrier layer (as required for Cu), as it not a deep level impurity, further simplifying the process and reducing its cost. One veteran method which has re-emerged is metal plating, with recent work demonstrating its viability [2]. Checking on Dimensions [3] shows that since the time of peak interest during 2012 there are on average 600 annual publications concerning using aluminum for front metallization of solar cells. As we have seen Al is inferior to Ag and Cu concerning its resistivity adding to a significant power efficiency loss due to series resistance resulting from the bus bars and fingers on the front side of the cell. Therefore further study is required in order to reduce the resistance of the Al front conductors. Lapovok et al. [1] demonstrated a 3.7% improvement (reduction) in resistivity from $\rho = 2.96 \mu\Omega \cdot cm$ to $\rho = 2.85 \mu\Omega \cdot cm$ following annealing at $600^\circ C$ for 48h. Following a similar treatment in a boron rich environment resulted in the resistivity dropping to $\rho = 2.62 \mu\Omega \cdot cm$ i.e. a 11.5% in resistivity which is a significant improvement. This increase was attributed to reduced scattering centers due to a gettering effect and reduced defects due to the additional annealing. Increasing the layers height resulting in an increase of the conductors cross section may assist in reducing the series resistance though the geometry may need some redesigning to avoid shadowing. Thus understanding mechanisms of electrical conduction in single crystals can lead to methods for reducing the electrical resistance of the front solar cell conductors. Ultra-high-purity aluminum single crystals are a good starting point for such experimental work, and high resolution X-ray diffraction, a measurement technique for assessing crystal quality and defects. However, it

*Corresponding author, gilad.orr@ariel.ac.il

is yet a significant challenge to determine the degree of crystalline perfection that will provide the optimal conditions for a significant improvement compared to the current accepted values. Every stage of the fabrication process has to be considered for its contribution to defect formation and elimination. Growing Aluminum single crystals was mostly investigated during several decades at the mid of the 20th century [4] by the well-known Bridgman method [5] or by using the grain growth technique. Recently, some new methods have



Figure 1. Bridgman based growth furnace with an inert growth environment

been applied for growing single crystal foils of several metals [6] that can be used at an industrial scale. Yet, the deformation in the crystals was mostly studied by intentional stressing of the crystal in order to perform the deformation, as well as studying the effects of heat treatment and annealing processes and characterize the resulting microstructure by means of X-ray diffraction methods and high-resolution microscopy [7]. The crystal orientation is precisely determined and oriented to the required direction, mostly to the $\{1,1,1\}$, $\{1,1,0\}$ or $\{1,0,0\}$ by the X-ray Laue method. This is followed by further XRD analysis for both final precise crystallographic orientations, as well as an initial assessment of the crystalline quality and microstructure. X-Ray Rocking Curve technique is applied in case of high crystalline quality assessment. Imaging methods such as optical microscopy, SEM and STEM, are carried out as well, for determining the physical microstructure that plays a significant role at the final X-Ray analysis. XRD peak shift, peak broadening and peak asymmetry are indicative of deformation, growth fault, twin fault and

several additional crystalline disorders in the FCC metal element crystal (Aluminum single crystal in the current study). Detailed theoretical calculations and experimental results are described in [8]. The FCC structure is a closed packed structure in which the atoms are arranged in a three layer sequence resulting in a dense geometric packing. Figure 2 illustrates a 3D arrangement of three such layers.

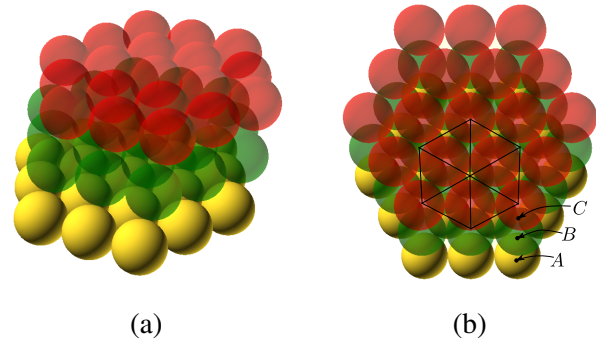


Figure 2. Representation of layers forming the FCC structure. (a) The recurring layer placement required for the FCC structure. (b) The actual location of the atoms missing the apex atom which is part of a top A layer (not shown).

The figure illustrates the layers of the atoms and the relative placement of each layer providing for the most compact filling. In Fig. 2b the orientation of the FCC cell within the 3 layer framework is shown. As the image is missing a top A layer the apex atom is missing. The cell structure is a bit obscure and one has to imagine the structure from the vertices. Figure 3 elucidates the FCC cell within the layers.

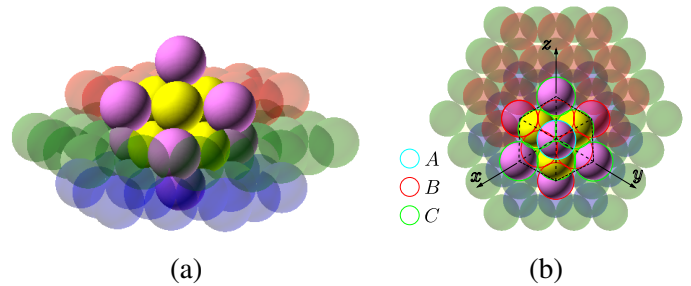


Figure 3. A FCC unit cell within the layers. (a) Side view of the FCC cell, (b) View of the cell from the $\{1,1,1\}$ direction.

The vertices atoms are illustrated by the violet spheres while the face centered atoms by the yellow spheres. As may be seen the apex atom and the bottom atom belong to the A layer placing them one over the other. Following the perpendicular unit cell axis one can observe the $\{1,1,1\}$ orientation in Figure 3b. The red bordered atoms highlight the vertex and face atoms at the lower layer, while the green bordered atoms highlight the ones of the layer above it. The vertices atoms of each layer form a large triangle bordering a smaller triangle created by the face atoms of that specific layer, with the smaller

triangle being at a 180° angle to the one formed by the vertices. The triangles formed by the atoms in each layer are a mirror image of the other. Given we had a perfect crystal, processing it mechanically will introduce defects. Point defects having less long range influence on the crystals structure. On the other hand, layer movement along the slip planes due to stress, with the primary ones being along the $\{1,1,1\}$ direction have much more influence for e.g. the line defects, the edge and screw dislocations. More subtle, but of significant influence on the diffraction patterns, are the stacking faults resulting in fault lines Fig. 4 and twins Fig. 5

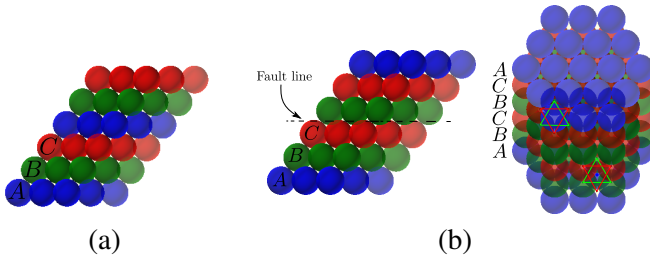


Figure 4. Layer stacking with a missing layer. (a) Regular 3 layer compact stacking resulting in the FCC structure. (b) Missing A layer (for example), resulting in the FCC cells missing the top or bottom atom creating a fault line.

Stacking faults in which one layer is missing, results in an alternating sequence of two layered stacks which result in a hexagonal closed packed structure along that layer. It could also be viewed as the top and bottom FCC cells missing one apex or base atom. Another stacking fault is when two adjacent layer switch positions as in Fig. 5

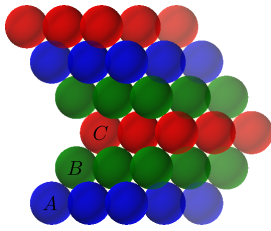


Figure 5. Layer stacking fault where two adjacent layers switch positions. This results in a bifurcation where the layers above the fault are a mirror image of the layers below it.

Such an occurrence leads to a bifurcation with the layers on both sides of the fault proceed as mirror images of one another prompting the growth of two crystals with a common layer in two different directions. Such a fault may have a considerable effect on the peak broadening. As we are dealing with single crystals we do not expect to observe grain boundaries, but low angle tilt boundaries resulting from dislocations and faults are present and its correlation with the rocking curve peak broadening in a manner not yet fully understood. They are observed using STEM imaging as can be seen in Fig. 6.

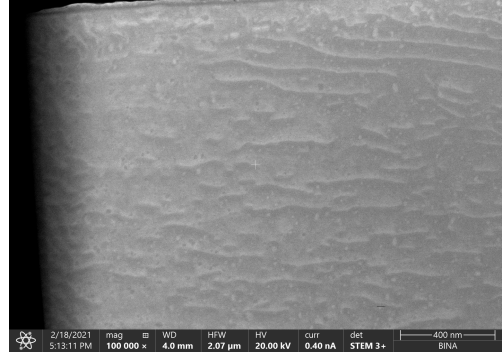


Figure 6. A $\times 80,000$ STEM image of low angle tilt boundaries, creating what is referred to as mosaic structures in aluminum.

Those boundaries differ from grain boundaries as from their very essence the bulk has a growth orientation and only locally differ from this orientation due to a periodic array of dislocations and stacking faults. The degree of this misorientation may be observed by the rocking curve method and in future published work will be correlated with the electrical conductivity in aluminum.

II. EXPERIMENTAL RESULTS

Following the Bridgman crystal Growth of Aluminum single crystals, samples were prepared for the purpose of crystallographic orientation, XRD analysis, X-Ray Rocking Curve analysis and crystalline quality evaluation by STEM imaging. As the material is very soft and ductile initial fabrication was conducted using electro-erosion. Figure 7 illustrates the result of an aluminum sample after it was cut. The STEM image displays the highly damaged top surface as observed in figure 7, which reduces the X-Ray intensity and increases the peak broadening.

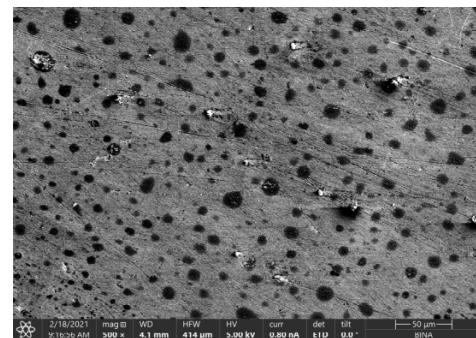


Figure 7. SEM image of the aluminum surface after cutting. The high pitting density, with the pit sizes reaching 20nm.

ICP-AES measurements indicated that trace elements of brass exist in the samples. Table I illustrates the trace elements within a sample compared to the trace elements found within the starting material and reference. Post EDM cutting displays obvious incorporation of brass

	Ag	Ca	Cu	Fe	Mg	Zn	Cr	S
Starting material	3.914	-	-	6.06	-	-	-	1282
Reference	3.98	-	-	6.45	-	-	0.12	87.59
Al EDM cut	-	13249	49506	14141	13.02	17064	0.66	-

Table 1

ICP-AES RESULTS OF SEVERAL SAMPLES (PPM)

elements into the crystal material. Following this SEM imaging, a STEM sample was prepared using a FIB process with the cut perpendicular to the observed surface in Fig. 7.

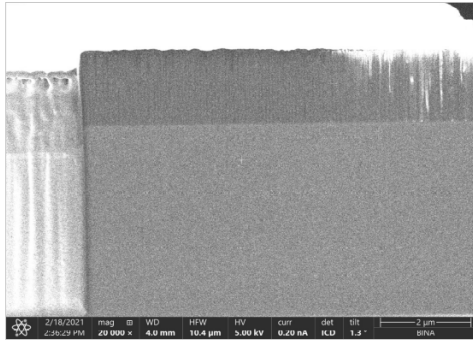


Figure 8. A low resolution STEM cross section image of the sample close to its surface. The damage to the machined layer can be clearly see, having the approximate thickness of $1.8\mu m$.

A magnified higher resolution STEM image (Fig. 9), displays column structure (“membrane like”) cavities with diameters corresponding to the previous pits observed in figure 7.

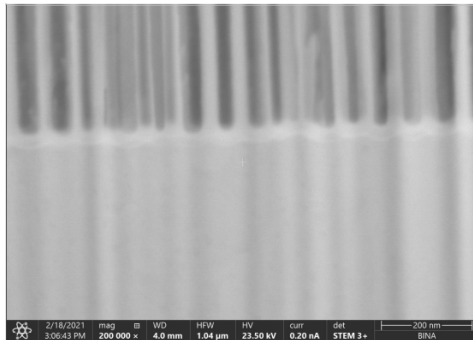


Figure 9. High resolution STEM image of the lamella prepared using the FIB technique

The image illustrates how the surface damage extends deep into the material altering its structure. This damage was found to propagate to a depth of approximately 2 mm with similar results reported in the past by Gorman et. al. [9]. Such damage results in reduced XRD intensity and considerable peak broadening. Those defects within the aluminum and on its external surfaces scatter conducting electrons and contribute to the resistivity. As the dimensions of the conductors are reduced, which is the case in the solar cell, the electrons interacting with the defects increase considerably resulting in a rise in resistivity. Figure 10 below, illustrates an example

of the XRD data that was acquired from a crystal with relatively poor quality. As may be observed, the diffraction pattern shows low peak intensity and mixed crystallographic orientation data.

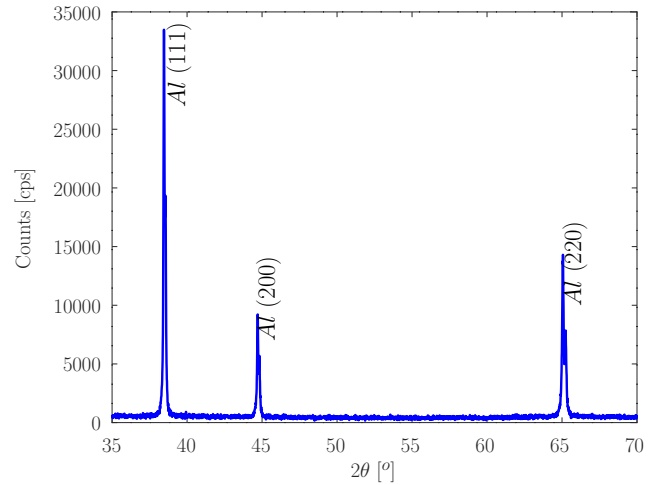


Figure 10. An example of $\{1,1,1\}$ oriented Aluminum Crystal. Minor diffraction at the $\{2,0,0\}$ and $\{2,2,0\}$ orientations are also visible.

Figure 11 below, shows an example of the XRD data that was acquired from a crystal of high quality and lattice perfection. A very high peak intensity at the range of $9e7$ (20 millions counts), with a single distinguished peak (disregarding K_β) diffraction in the $\{1,1,1\}$ crystallographic orientation.

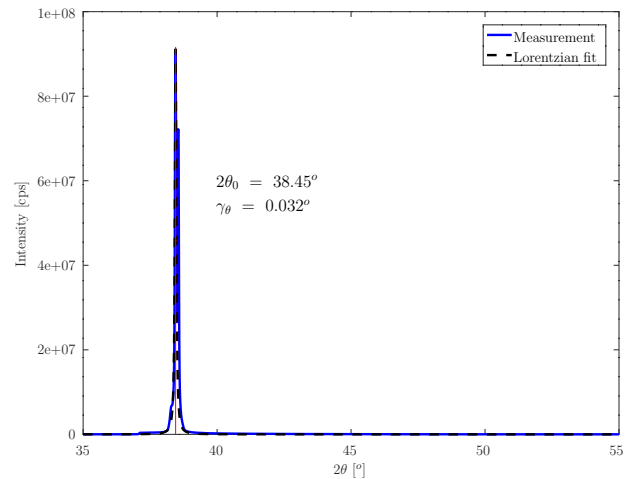


Figure 11. An example of an XRD chart for a precisely oriented Aluminum Crystals in the $\{1, 1, 1\}$ direction.

Next, figure 12 shows the Rocking Curve peak, with a FWHM of about 0.36 degrees, yet, it should be noted that the RC shape exhibits a minor asymmetry, indicating on some crystalline in-homogeneity. As can be seen in the figure, there is an axial divergence at the lower angles of the peak, causing asymmetry. This asymmetry is an indication of an anisotropic strain.

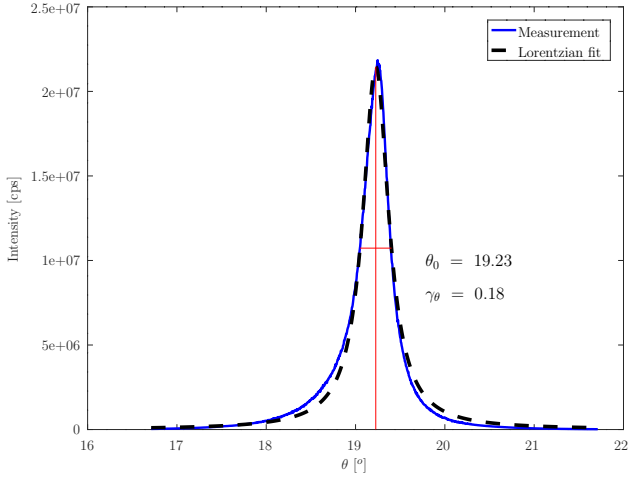


Figure 12. An example of an X-Ray Rocking Curve chart, with a FWHM of about 0.36 degrees and very high peak intensity in the range of $2e7$, a slight asymmetry is evident as well.

The results were fit using a Lorentz (Cauchy) PDF (probability distribution function), that was found to better fit the results. If we take the Lorentzian's FWHM as a measure of orientation spread of the mosaic structure tilt, we can estimate that it is approximately 0.18° . Following the FWHM angle spread of the tilt angles we can calculate the upper limit of the dislocation density [10].

$$D = \frac{(FWHM/2)^2}{9b^2} = \frac{\gamma_\theta^2}{9b^2} \quad (1)$$

where γ_0 is the tilt spread, and b is the Burgers vector. For the aluminum with an FCC structure in the (1,1,1) direction, the Burgers vector is given by

$$b = \frac{a}{2} \cdot \sqrt{(h^2 + k^2 + l^2)} = \frac{a\sqrt{3}}{2} \quad (2)$$

where a is the side length of the unit cell. As it is $4.046 \times 10^{-10} m$, $b = 3.504 \times 10^{-10} m$. Thus the upper limit estimate of the dislocation density is

$$D = 8.93 \times 10^8 [cm^{-2}]$$

which is considered high compared to work published by Mizuno Et al. [11]. This is reasonable as in the mentioned work, ultra high purity raw materials were used (7N), the samples were thin with an elaborate annealing process. Considering the stress within the crystal, we could expect that the stress is non uniform. This was evident by rocking curve mapping resulting in different tilt spreads as can be seen in Figure 13.

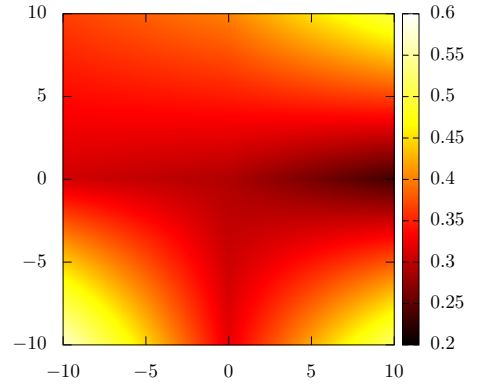


Figure 13. Rocking curve mapping of the tilt spread on a 2x2 cm area from a crystal cross section.

as the tilt spread is correlated to the dislocation density which is further correlated to the stress, it shows the non uniform stress within the sample. This must reflect on the peak intensity (counts) as shown in Figure 14.

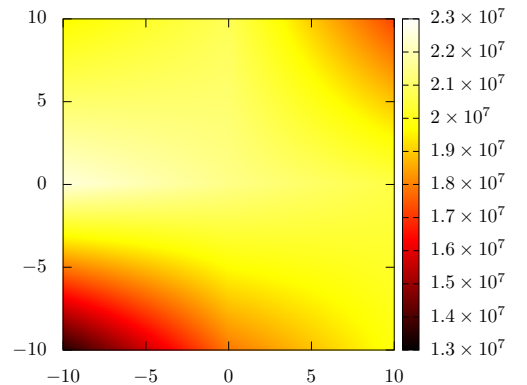


Figure 14. Rocking curve mapping of peak intensity on a 2x2 cm area from a crystal cross section

While the XRD rocking curve angle spread is an average of many low tilt angle subgrains, being macroscopic in nature, the fine structure can be observed using STEM imaging. Figures 15a and 15b, illustrate the STEM results displaying the dislocation defects in a crystal that exhibits sub grain boundaries (low angle) within grains, and tilt boundaries that may significantly differ from each other.

III. CONCLUSIONS

X-ray diffraction methods and Rocking-curve analysis, supported by SEM and STEM imaging, were shown to display, in an effective manner the three dimensional crystalline quality of aluminum single crystals. This

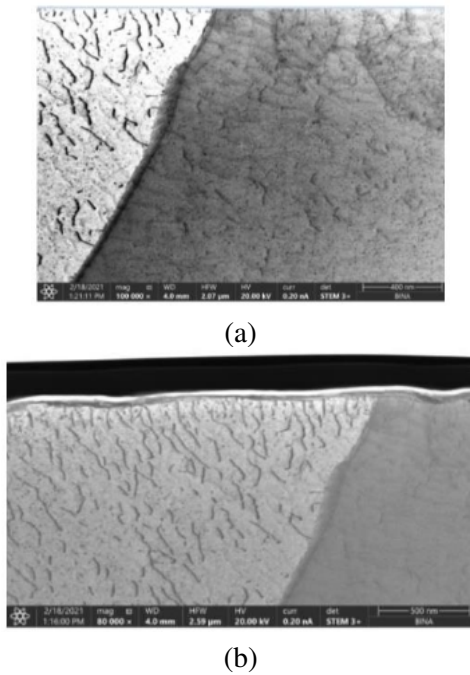


Figure 15. (a) is a STEM image of an Aluminum crystal with high defect density, reflected at the observed sub grains and dislocation defects. (b) Shows displays the native oxide layer of the surface of the crystal.

is demonstrated with both poor and high quality aluminum single crystals grown using the veteran Bridgman method. Growth and fabrication of the crystals were still found to be short of the strived state of the art. It was further demonstrated that sample fabrication by rough electro-erosion cutting, exhibited a membrane like, porous deformed structure at the aluminum as cut surface. Supplementing electrical conductivity measurements of aluminum, quality assessment of defects in front cell aluminum conductors can assist in designing novel low resistance aluminum conductors replacing the currently widely used and relatively rare silver.

REFERENCES

- [1] Rimma Lapovok, Yaron Amouyal, Yuanshen Qi, Alex Berner, Anna Kosinova, Eugene Lakin, Dmitri A Molodov, and Emil Zolotoyabko. Enhancement of electrical conductivity in aluminum single crystals by boron treatment in solid state. *Journal of Materials Science*, 55(6):2564–2577, 2020.
- [2] Lewis Ricci, Mao-Feng Tseng, Meng Tao, Yunyu Liu, Fangdan Jiang, and Guoqiang Xing. Light-induced al plating on si for fabrication of an ag-free all-al solar cell. *ECS Journal of Solid State Science and Technology*, 10(2):025004, 2021.
- [3] Dimensions solar cells front aluminum metallization, 2021. Accessed: 2021-07-11.
- [4] SK Mohanlal and D Pathinettam Padiyan. Crystal growth of aluminium by two simple methods.

- Journal of Physics D: Applied Physics*, 15(2):L11, 1982.
- [5] S Zerbib, G Orr, and G Golan. Open top seeding crystal growth control system. *BULGARIAN CHEMICAL COMMUNICATIONS*, page 85, 2020.
- [6] Sunghwan Jin, Ming Huang, Youngwoo Kwon, Leining Zhang, Bao-Wen Li, Sangjun Oh, Jichen Dong, Da Luo, Mandakini Biswal, Benjamin V Cuning, et al. Colossal grain growth yields single-crystal metal foils by contact-free annealing. *Science*, 362(6418):1021–1025, 2018.
- [7] DML Bartholomew and A Hellawell. Changes of growth conditions in the vertical bridgman-stockbarger method for the solidification of aluminum. *Journal of Crystal Growth*, 50(2):453–460, 1980.
- [8] Bertram Eugene Warren. *X-ray Diffraction*. Courier Corporation, 1990.
- [9] JA Gorman, DS Wood, and T Vreeland Jr. Mobility of dislocations in aluminum. *Journal of Applied Physics*, 40(2):833–841, 1969.
- [10] PBKA Gay, PB Hirsch, and A Kelly. The estimation of dislocation densities in metals from x-ray data. *Acta metallurgica*, 1(3):315–319, 1953.
- [11] Kaoru Mizuno, Satoshi Yamamoto, Kimihiko Morikawa, Masanori Kuga, Hiroyuki Okamoto, and Eiji Hashimoto. Vacancy generation mechanism at high temperatures in ultrahigh-purity aluminum single crystals with a low dislocation density. *Journal of Crystal Growth*, 275(1-2):e1697–e1702, 2005.